Gapless spin-liquid state in the structurally disorder-free triangular antiferromagnet NaYbO2

Lei Ding, Pascal Manuel, Sebastian Bachus, Franziska Grußler, Philipp Gegenwart, John Singleton, Roger D. Johnson, Helen C. Walker, Devashibhai T. Adroja, Adrian D. Hillier, Alexander A. Tsirlin

Angaben zur Veröffentlichung / Publication details:

Ding, Lei, Pascal Manuel, Sebastian Bachus, Franziska Grußler, Philipp Gegenwart, John Singleton, Roger D. Johnson, et al. 2019. "Gapless spin-liquid state in the structurally disorder-free triangular antiferromagnet NaYbO2." *Physical Review B* 100 (14): 144432. https://doi.org/10.1103/physrevb.100.144432.

Editors' Suggestion

Gapless spin-liquid state in the structurally disorder-free triangular antiferromagnet $NaYbO_2$

Lei Ding,[1,*] Pascal Manuel,[1] Sebastian Bachus,[2] Franziska Grußler,[2] Philipp Gegenwart,[2] John Singleton,[3] Roger D. Johnson,[4] Helen C. Walker,[1] Devashibhai T. Adroja,[1,5] Adrian D. Hillier,[1] and Alexander A. Tsirlin[2]

[1]*ISIS Facility, Rutherford Appleton Laboratory, Harwell Oxford, Didcot OX11 0QX, United Kingdom*

[2]*Experimental Physics VI, Center for Electronic Correlations and Magnetism, University of Augsburg, 86135 Augsburg, Germany*

[3]*National High Magnetic Field Laboratory, Los Alamos National Laboratory, Los Alamos, New Mexico 87545, USA*

[4]*Clarendon Laboratory, Department of Physics, University of Oxford, Oxford OX1 3PU, United Kingdom*

[5]*Highly Correlated Matter Research Group, Physics Department, University of Johannesburg, Auckland Park 2006, South Africa*

(Received 21 January 2019; revised manuscript received 4 October 2019; published 24 October 2019)

We present a candidate material, $NaYbO_2$, that realizes the genuine spin-liquid state on the triangular lattice and benchmarks recent theoretical predictions on the relevant spin models. Synchrotron x-ray diffraction and neutron scattering exclude both structural disorder and crystal-electric-field randomness. Our thermodynamic measurements, neutron diffraction, and muon spectroscopy coincidentally prove the absence of magnetic order and persistent spin dynamics down to at least 70 mK. Continuous magnetic excitations first observed by inelastic neutron scattering show a gapless feature and the low-energy spectral weight accumulating at the K point of the Brillouin zone, in agreement with theoretical predictions for the spin-liquid phase of triangular antiferromagnets. Such a gapless spin-liquid phase is further confirmed by our magnetic specific heat analysis that reveals a departure from simple power-law behavior. Our work demonstrates that $NaYbO_2$ practically gives direct experimental access to the spin-liquid physics of triangular antiferromagnets.

DOI: 10.1103/PhysRevB.100.144432

I. INTRODUCTION

Quantum spin liquids (QSLs) in frustrated magnets have attracted a lot of attention because of the occurrence of unconventional ground states, where highly entangled spins and their strong fluctuations are observed in the absence of long-range order down to zero temperature. The ensuing excitations are interesting in their own right as they are distinct from magnons in systems with conventional long-range magnetic order [1–3]. Historically, the QSL state was first exemplified by the nearest-neighbor resonating-valence-bond state on the triangular lattice (TL) [4], which has drawn a great deal of interest in the TL ever since, although the majority of real-world triangular materials order magnetically at low temperatures [5].

Recently, a promising QSL candidate, $YbMgGaO_4$, with the effective spin-1/2 Yb^{3+} ion on the TL was proposed by Li *et al.* [6,7]. They observed persistent spin dynamics down to at least 48 mK [8] and the $T^{0.7}$ power-law behavior of the specific heat [6], indicative of the gapless U(1) QSL characterized by a Fermi surface of fractionalized (spinon) excitations. Although continuous spinonlike excitations were indeed observed experimentally [9], their assignment to spinons [10] is far from unambiguous, and alternative phenomenological explanations within the valence-bond framework were proposed as well [11–13]. Moreover, an absent magnetic contribution to the thermal conductivity [14], considerable broadening of spin-wave excitations in the fully polarized state [15], and acute broadening of the crystal-electric-field (CEF) excitations of Yb^{3+} [16] reveal a significant complexity in this material. The problem appears to be related to the statistical distribution of Mg^{2+} and Ga^{3+} that randomizes the local environment of Yb^{3+} [16] and may lead to peculiar effects like spin-liquid mimicry [17,18], although the exact influence of the structural randomness (disorder) on the magnetic parameters remains debated [19]. Whether or not these structural effects are integral to the spin-liquid formation, the complexity of $YbMgGaO_4$ hinders its use as a reference model material for the QSL state in the TL.

On the theory side, significant efforts were made to establish the parameter regime where long-range magnetic order gives way to a QSL [20–22]. Whereas nearest-neighbor Heisenberg interactions J_1 on the TL support the 120° magnetic order [23], a weak second-neighbor coupling J_2 is sufficient to suppress this order and drive the system toward a QSL state [24–31]. The presence of multiple anisotropic interactions–a characteristic of the Yb^{3+} compounds–lays out another route to the QSL [21,32–35]. These two regimes, the second-neighbor isotropic exchange vs nearest-neighbor anisotropic exchange, may, in fact, produce isomorphic QSL phases, as suggested in a recent theoretical work [32], where it was shown that these phases are either Z_2 or Dirac-like, while discarding the spinon-metal scenario originally proposed for $YbMgGaO_4$. Despite these recent achievements, the exact nature of the QSL phases and even the presence [26,30] or absence [24,27,28] of a spin gap therein remain vividly debated. Experimental input is thus highly desirable but requires a disorder-free material characterized down to millikelvin temperatures, as magnetic interactions in the Yb^{3+} oxides are of the order of 1 K, and the ground-state regime is practically reached only below 0.4 K [6,8].

*lei.ding.ld@outlook.com

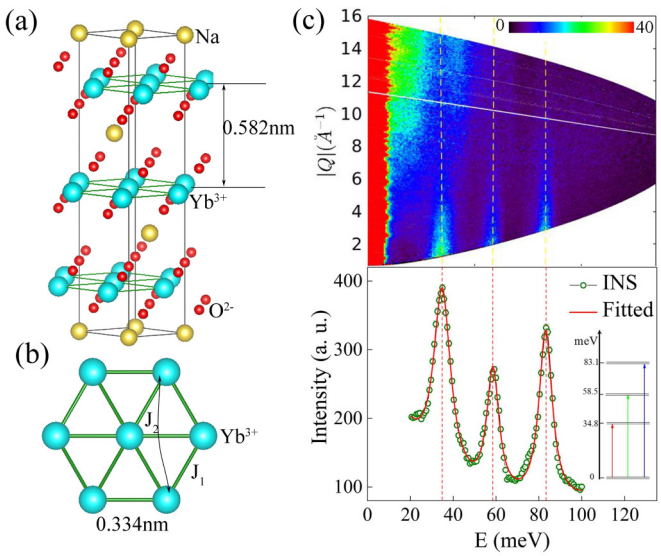

FIG. 1. (a) Stacking of the Yb^{3+} triangular layers along the c axis. (b) Triangular layer formed by Yb^{3+} cations. (c) Inelastic neutron scattering spectra $S(Q, \hbar\omega)$ at 5 K with $E_i = 150$ meV. Energy dependence of the INS intensity at 5 K integrated in Q over the range 3.9−4.4 $Å^{-1}$. The inset depicts the CEF transitions from the ground-state Kramers doublet.

Na-based chalcogenides $NaYbX_2$ (X = O, S, Se) have recently come to the attention of researchers as ideal triangular antiferromagnets [36,37]. They feature layers of edge-sharing YbO_6 octahedra with the triangular arrangement of the magnetic Yb^{3+} ions. These layers are separated by the well-ordered Na atoms, with an interlayer Yb-Yb distance of 5.82 Å, which is shorter than in $YbMgGaO_4$ (8.61 Å) but still significantly longer than the nearest-neighbor Yb-Yb distance of 3.34 Å within the triangular planes [see Figs. 1(a) and 1(b)].

Here, we confirm the absence of chemical site disorder and report persistent spin dynamics in $NaYbO_2$ down to at least 70 mK. We also observe continuous excitations that are qualitatively similar to those predicted [32] for the QSL state in the TL. Our results set up $NaYbO_2$ as a disorder-free spin-liquid candidate and shed light onto the physics of the spin-liquid state in the TL. We demonstrate the gapless nature of this state and the absence of simple power-law scaling for the specific heat.

II. METHODS

Sample preparation. Polycrystalline $NaYbO_2$ was synthesized by a solid-state reaction. The mixture of high-purity reagents Na_2CO_3 and Yb_2O_3 with the molar ratio 2.5:1 was ground in an agate mortar and pelletized. The pellets were placed into alumina crucibles and heated in air at 900 °C for 20 h and cooled down to room temperature. The obtained sample was washed by distilled water and ethanol and then dried in air at room temperature for 2 days.

Synchrotron x-ray and neutron diffraction. The crystal structure and quality of the powder sample was checked by high-resolution synchrotron x-ray diffraction (SXRD) and neutron diffraction. SXRD data were collected at the ID22 beamline of the European Synchrotron Radiation Facility (ESRF), France, with a wavelength of $\lambda = 0.35456$ Å at 10 K and at 250 K. The sample was placed into a thin-wall glass capillary and spun during the measurement. Diffracted intensity was recorded by nine scintillation detectors, each preceded by a Si(111) analyzer crystal. The neutron powder diffraction data were collected at the ISIS pulsed neutron and muon facility of the Rutherford Appleton Laboratory (United Kingdom) on the WISH diffractometer located at the second target station [38]. A powder sample (∼2 g) was loaded into a 6-mm-diameter cylindrical vanadium can and measured in the temperature range of 1.5–100 K using an Oxford Instrument cryostat. The data at various temperatures were collected for 1 h. The neutron experiment at 90 mK was performed in a dilution fridge equipped with a capillary with the powder sample encapsulated in a copper can.

Neutron scattering for the crystal electric field. High-energy inelastic neutron scattering (INS) spectra were collected on the MERLIN spectrometer at the ISIS facility with incident energies $E_i = 90$ and 150 meV at 5 and 300 K [39]. A vanadium can with the ∼5.4-g powder sample was loaded in a closed-cycle refrigerator system.

Magnetization characterization. The magnetic properties of $NaYbO_2$ were investigated by combining steady and pulsed magnetic fields. The temperature-dependent magnetic susceptibility was measured from 0.4 to 2 K in the zero-field-cooled (ZFC) procedure and from 1.8 to 350 K in ZFC and field-cooled (FC) procedures using a superconducting quantum interference device magnetometer (Quantum Design, MPMS-7T) under various magnetic fields. The magnetic susceptibility with field up to 16 T was measured using a Quantum Design physical property measurement system (PPMS) fitted with the vibrating sample magnetometer option. The field-dependent magnetization up to 65 T was measured at 0.45 K using a triply compensated extraction magnetometer within a 65-T short-pulse magnet at the National High Magnetic Field Laboratory, Los Alamos, New Mexico.

Heat capacity measurements. The specific heat was measured on a pressed pellet of $NaYbO_2$ using the PPMS from Quantum Design with the ^{3}He insert (above 0.4 K) and a home-built setup installed in the dilution-fridge cryostat (0.07–2.0 K). Specific heat of $NaYbO_2$ was determined by using the thermal relaxation method, where the response of the sample temperature $T(t)$ is measured after applying a heater power ΔP [40].

Zero-field and longitudinal-field muon spectroscopy. The muon spectroscopy measurements were carried out on the MuSR spectrometer at the ISIS facility using zero-field (ZF) and longitudinal-field (LF) options. The sample was mounted on a high-purity silver plate, which gives only a nonrelaxing background signal. Temperatures down to 0.1 K were achieved by using a dilution refrigerator.

Neutron scattering for the low-energy excitations. Low-energy excitations of $NaYbO_2$ were measured at the cold-neutron multichopper LET spectrometer (ISIS) [41] at 0.045, 0.3, 0.6, 10, 30, 50, 80, and 100 K using incident neutron energies of 1.46, 3.7, and 7.52 meV. The lowest incident energy of 1.46 meV leads to an instrument resolution of about 0.02 meV. This enables us to probe the low-energy spin excitations that usually come as a big challenge in many investigations

but provide clear evidence for the type of magnetic ground state.

III. RESULTS

A. Crystal structure and crystal-electric-field excitations

Both x-ray and neutron diffraction data confirm that $NaYbO_2$ crystallizes with *R*-3*m* symmetry (see Fig. 1). The absence of chemical site disorder was verified by synchrotron x-ray and neutron diffraction data [40] collected in the temperature range of 90 mK to 300 K. No signature of site deficiency (less than 1% for the Na and O sites) or disorder was observed in the structure refinements performed down to 90 mK [40] using the FULLPROF software [42]. The high-resolution synchrotron XRD data reveal very sharp peaks and rule out any extended defects that may occur in a layered compound [40]. At 10 K, the atomic displacement parameter of Yb is below 10^{-3} Å^2 and excludes any off-center displacements that have been the most direct signature of structural randomness in $YbMgGaO_4$ [16]. Neutron diffraction data collected at 90 mK do not show any magnetic Bragg peak, indicating the absence of any long-range magnetic order in $NaYbO_2$ [40].

In $YbMgGaO_4$, the structural disorder becomes most conspicuous in the CEF excitations that broaden and even show four peaks in the inelastic neutron spectrum [16], instead of the three peaks expected for Yb^{3+} with its $^2F_{7/2}$ multiplet split into four Kramers doublets by the trigonal crystal field [43,44]. The CEF excitations of $NaYbO_2$ were measured at 5 K with incident energies of 90 and 150 meV. As shown in Fig. 1(c), three sharp, resolution-limited CEF excitations are observed, as expected for Yb^{3+}. This ultimately proves the absence of structural disorder in our material. In contrast to many previous QSL candidates, in particular the Yb-based $YbMgGaO_4$, our system does not appear to suffer from any significant structural disorder that could have influenced the magnetism of the $4f$ ions.

From the excitation energies and line intensities we extract the CEF parameters and the compositions of the four Kramers doublets [40] using the MANTID software[45]. It is worth noting that the excitation energies of 34.8, 58.5, and 83.1 meV are not far from those reported for $YbMgGaO_4$ (39.4, 61.3, and 96.6 meV, respectively [16]) excluding the shoulder at 87 meV. This proximity of the CEF energies reflects similar local environments of Yb^{3+} in both compounds. $NaYbS_2$ was found to show all its CEF excitations below 50 meV, although the data remained inconclusive because additional unexpected peaks, presumably caused by a massive impurity phase, were observed [36]. Therefore, our data on $NaYbO_2$ provide reliable results on CEF excitations for Yb^{3+} in the delafossite compound family. Similar CEF excitations in $YbMgGaO_4$ and $NaYbO_2$ indicate that on the level of single-ion physics the latter can be seen as a close analog of the former, but with the structural disorder completely removed.

B. Thermodynamic properties

At low temperatures, the magnetic behavior of $NaYbO_2$ is fully determined by the ground-state Kramers doublet and can be described by an effective pseudospin-$\frac{1}{2}$ Hamiltonian [46]. However, the higher-lying CEF levels produce a sizable

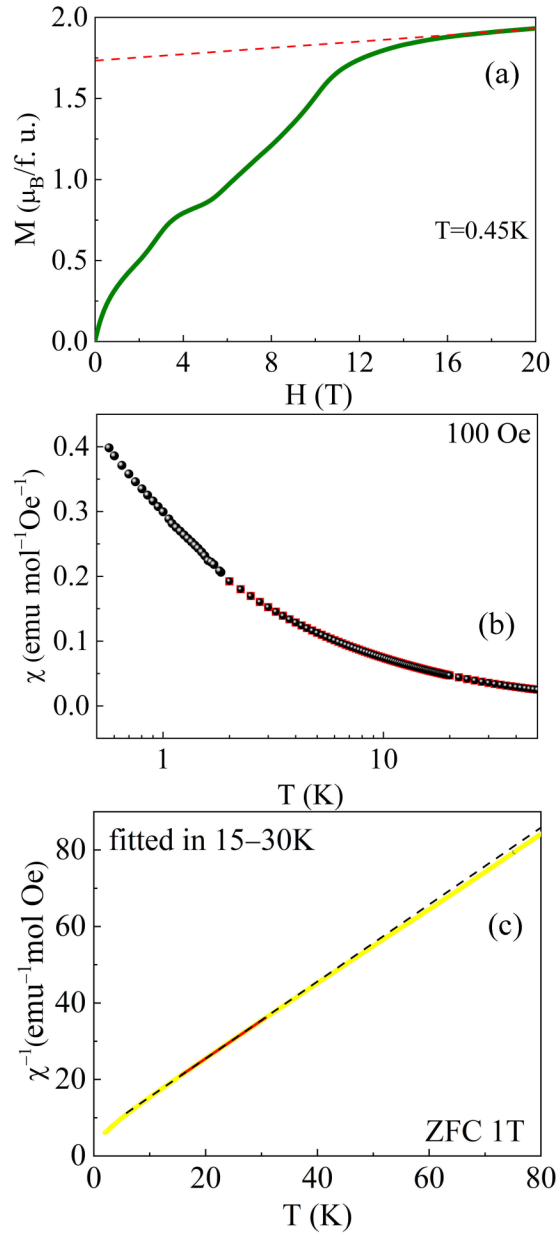

FIG. 2. (a) Isothermal magnetization curve measured at 0.45 K up to 60 T. The red line marks the Van Vleck contribution. (b) Temperature dependence of the magnetic susceptibility of $NaYbO_2$ down to 0.4 K. ZFC and FC curves are shown down to 1.8 K. (c) The Curie-Weiss fit to the inverse magnetic susceptibility in the range of 15–30 K after subtracting the Van Vleck term.

Van Vleck term χ_{vv}. To determine the χ_{vv}, we measured field-dependent magnetization at 0.45 K using a triply compensated extraction magnetometer within a 65-T short-pulse magnet. As shown in Fig. 2(a), $NaYbO_2$ saturates at around 16 T. The magnetization increases linearly in higher fields, and its slope corresponds to a Van Vleck term of $\chi_{vv} = 0.0101\mu_B/T = 0.00564\,\text{emu mol}^{-1}\,\text{Oe}^{-1}$ [40]. After subtracting this Van Vleck contribution, we arrive at the saturation magnetization of 1.75 μ_B/f.u., which compares favorably to 1.5 μ_B/f.u. expected from the powder-averaged $\bar{g} = 3.00$ calculated based on the CEF fit. Before going further, we note in passing

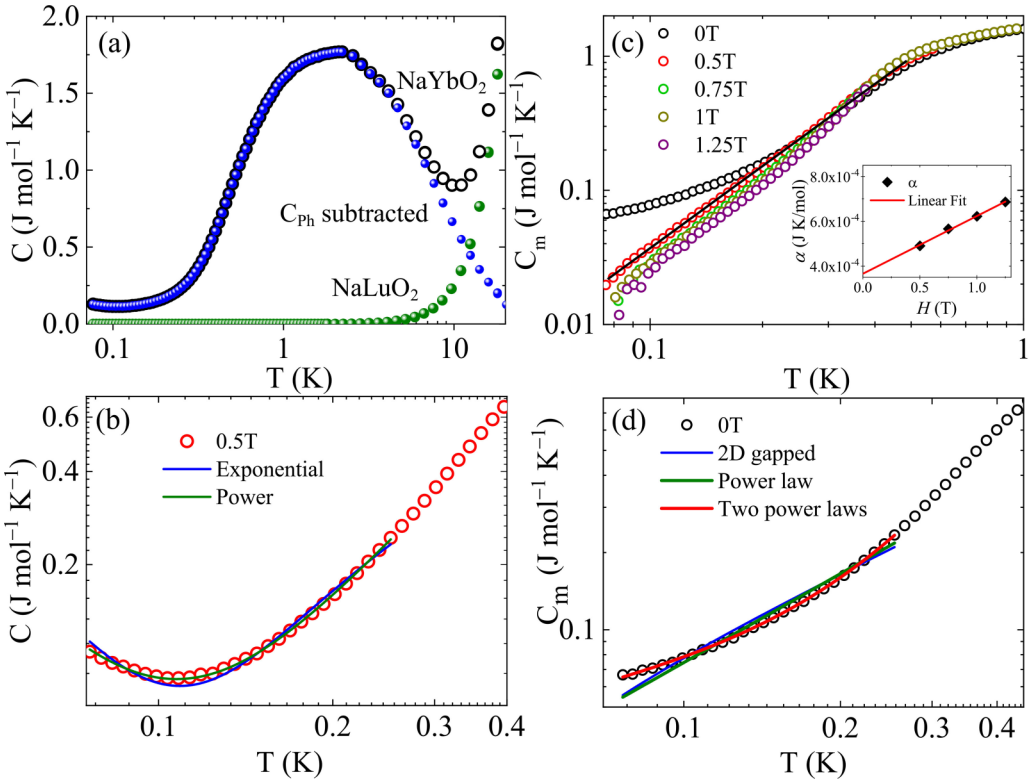

FIG. 3. (a) Specific heat data for $NaYbO_2$ and the nonmagnetic reference $NaLuO_2$. They show that the lattice contribution below 2 K is negligible. (b) Example for the fit of the raw specific heat data in order to determine the nuclear contribution $C_{\rm nucl}$. (c) The magnetic contribution $C_m = C - C_{\rm nucl}$ of the specific heat of $NaYbO_2$ in a double-logarithmic plot in low magnetic fields after subtracting the nuclear contribution. The black line is a guide to the eye and shows that C_m follows a power law only if a magnetic field is applied. The zero-field data clearly deviate from that behavior. The inset shows the field dependence of parameter α and its extrapolation to zero field. (d) Zero-field magnetic specific heat of $NaYbO_2$ with fits using different functions.

that the magnetization curve of $NaYbO_2$ measured at 0.45 K shows a plateau between 4 and 5 T at about one half of the saturation magnetization, as shown in Fig. 2(a). Such a $\frac{1}{2}$ plateau that can appear at $\bar{J}_2/\bar{J}_1 > 0.125$ [47] contrasts with the $\frac{1}{3}$ plateau typically observed in Heisenberg and XXZ TLs [5] and may be indicative of a more complex interaction regime. Moreover, field-induced phase transitions occur in $NaYbO_2$ [48], but they go beyond the scope of our present report and will be addressed in future studies.

The magnetic susceptibility on $NaYbO_2$ was measured in the temperature range of 0.4–300 K under various magnetic fields [40]. As shown in Fig. 2(b), the curve increases monotonically with decreasing temperature and shows no magnetic anomaly down to 0.4 K under a magnetic field of 100 Oe. The bifurcation between the ZFC and FC curves, typically found in spin-glass systems, is absent in $NaYbO_2$. The inverse magnetic susceptibility shows a change in slope around 70 K, with the low-temperature linear part reflecting the Curie-Weiss behavior of pseudospins- $\frac{1}{2}$ [see Fig. 2(c)]. Magnetic susceptibility with χ_{vv} subtracted follows the Curie-Weiss law, which yields an effective moment of $\mu_{\rm eff} = 2.84(2)\mu_B$ and Curie-Weiss temperature $\Theta = -5.64(1)$ K. The former is close to the value of $2.60\,\mu_B$ expected from the powder-averaged $\bar{g} = 3.00$. The latter with a negative value reflects antiferromagnetic interactions between the Yb^{3+} pseudospins. It is worth noting that the absolute value is about two times larger than that in $YbMgGaO_4$ ($\Theta_\parallel = -1.5$ K, $\Theta_\perp = -2.7$ K [7]) and corroborates the twofold increase in the saturation field from 8 T in $YbMgGaO_4$ to 16 T in $NaYbO_2$. The simple estimate $\Theta = -3\bar{J}_1/2$ for a TL yields $\bar{J}_1 \simeq 3.8$ K, the energy scale of nearest-neighbor exchange couplings in $NaYbO_2$.

To probe low-temperature thermodynamics, we measured the specific heat C_p of $NaYbO_2$ using a home-built dilution-fridge setup down to 70 mK [40,49]. As seen in Fig. 3(a), the magnetic contribution to C_p becomes visible below 8 K and shows a broad maximum around 1 K. At even lower temperatures, the magnetic contribution decreases without showing any signature of a magnetic transition [see Fig. 3(d)]. These features suggest the absence of long-range magnetic order and the possibility of a spin-liquid state.

Magnetic specific heat is combined with other contributions. We confirmed that below 2 K the lattice contribution $C_{\rm Phon} = \beta T^3$ is negligible, as shown by comparing the heat capacity of $NaYbO_2$ to that of the nonmagnetic analog $NaLuO_2$ [Fig. 3(a)]. The contribution of free electrons should be null as white-colored $NaYbO_2$ is a typical insulator. The upturn of the specific heat below 150 mK is caused by the nuclear contribution $C_{\rm nucl}$ and can be described as the high-temperature part of a Schottky anomaly, $C_{\rm nucl} = \alpha/T^2$. Note that this contribution mainly arises from the Yb nuclei and cannot be corrected by simply subtracting the specific heat of $NaLuO_2$.

Moreover, it is present even in zero field, owing to the quadrupolar splitting of the Yb^{3+} nuclear levels. Therefore, one has to fit low-temperature specific heat with a suitably chosen model.

To construct such a model, we use the Schottky anomaly for $C_{\rm nucl}$ and consider the magnetic contribution $C_m(T)$ either in the exponential form, $a(T)e^{-\Delta/T}$ (where $a(T)$ is a temperature-dependent pre-factor for a gapped 2D antiferromagnet) [40], or in the form of a power law T^p to account for gapped and gapless excitations, respectively. In small applied fields, the heat capacity data below 250 mK can be well described by a combination of the nuclear Schottky anomaly and a $T^{2.2}$ power law, as exemplified in Fig. 3(b). On the other hand, the exponential term clearly fails to fit the data, suggesting the gapless nature of the low-energy excitations. The fitting parameters are summarized in Table S6 in the Supplemental Material [40].

The zero-field data prove to be more complicated, as neither the power-law nor the exponential forms of $C_m(T)$ fit the data [Fig. 3(d)]. To determine $C_{\rm nucl}$, we extrapolated the field dependence of α to zero field, arriving at $\alpha(0T) = 3.66 \times 10^4$ J K mol^{-1} [see the inset of Fig. 3(c)]. The remaining magnetic part $C_m(T)$ deviates from the simple power-law behavior indeed. We can tentatively fit it with two power laws, $aT^p + bT^q$, where $p \simeq 2.9$ resembles the T^3 contribution of magnons in a long-range-ordered antiferromagnet and $q \simeq 0.5$ reflects a sublinear behavior, which is remotely similar to the power-law behavior in $YbMgGaO_4$ [6], although this two-power-law analysis should not be taken as strong evidence of the presence of magnon excitations in $NaYbO_2$ because other combinations of fitting functions may account for the data as well. Theory input is strongly required to understand the exact nature of this unusual zero-field behavior. Here, we note only that the possible presence of two different contributions to $C_m(T)$ is intrinsic to the material and could not arise from sample inhomogeneity because even a weak applied field of 0.5–1.25 T restores the simpler $T^{2.2}$ power-law behavior [see Fig. 3(c)].

From the specific heat data we conclude that the low-energy excitations in $NaYbO_2$ are neither gapped nor magnonlike. They are also distinct from the low-energy excitations in $YbMgGaO_4$ that showed [6] the robust $T^{0.7}$ power-law characteristic of the "spinon metal" of a U(1) quantum spin liquid [50].

C. Muon spin relaxation measurement

Our heat-capacity data exclude long-range magnetic ordering above 70 mK, yet spin freezing would have no immediate effect on the specific heat. A direct probe of spin dynamics is thus essential to identify the QSL. To this end, we carried out ZF and LF muon spin relaxation (μSR) measurement down to 100 mK at the MuSR spectrometer.

Four representative ZF μSR spectra are shown in Fig. 4(a). They reveal neither oscillations nor a drastic drop in the initial asymmetry, indicative of the long-range magnetic order, but instead show signatures of persistent spin dynamics; in particular the lack of polarization recovery to $\frac{1}{3}$ of the initial value rules out the presence of static random fields. Initially, we fit the ZF spectra to a stretched exponential function, which

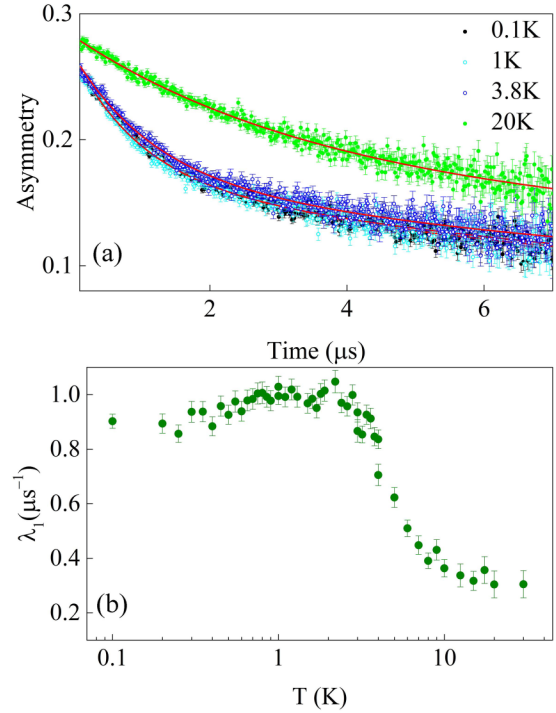

FIG. 4. (a) ZF μSR spectra collected at various temperatures. The solid lines represent the fit using function (1). (b) Temperature dependence of the muon spin relaxation rate for the ZF μSR spectra.

yields unsatisfactory agreement with our data. By inspecting the crystal structure of $NaYbO_2$, it is possible that the muons implanted could locate on two sites with different bonding between the bonds of Yb-O-Na. Such a configuration makes one of the muon sites close to Yb but the other more distant [40]. We thus further analyze these data by fitting the muon spectra with two exponential components:

$$A(t) = A_0[f_1 \exp(-\lambda_1 t) + (1 - f_1)\exp(-\lambda_2 t)] + B_0, \quad (1)$$

where $A_0 = 0.1917$ and $B_0 = 0.065$ denote the initial asymmetry and the constant background, respectively, λ_1 and λ_2 represent the muon spin relaxation rates for muons implanted at two sites near O^{2-}, and f_1 stands for the fraction of the first component. This function with two exponential components successfully reproduces the μSR data. Note the data analysis was carried out by considering the μSR data up to 15μs. The fitted ZF μSR relaxation rates λ_1 and λ_2 and f_1 as a function of temperature are shown in [40]. f_1 shows temperature-independent behavior with its value close to 0.5, suggesting the same population at the two muon sites. Below, we will discuss the electronic dynamics in terms of λ_1 since it is significantly larger than λ_2.

The temperature dependence of λ_1 tracks the onset of correlations between the Yb^{3+} pseudospins. As seen in Fig. 4(b), above 10 K, $NaYbO_2$ is paramagnetic with a smaller and temperature-independent λ_1. The increase in λ_1 below 10 K is accompanied by the growing magnetic contribution to the specific heat, whereas the second temperature-independent regime below 2 K may indicate a crossover toward the spin-liquid state. Such features are consistent with other spin-liquid

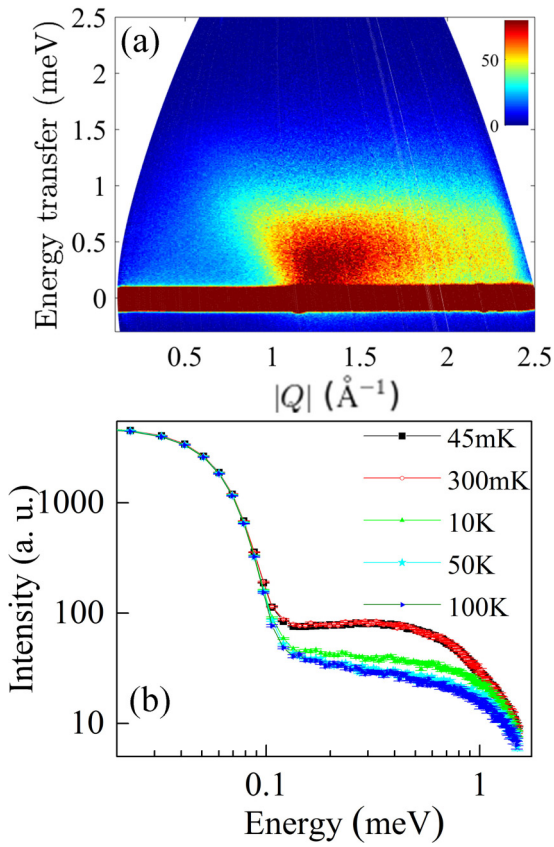

FIG. 5. (a) INS spectra measured at 45 mK with the incident energies $E_i = 3.7$ meV. (b) Energy dependence of the integrated cut along Q in the range of 1.2−1.5 Å^{-1}.

candidates. To prove the dynamic nature of the relaxation in this temperature range, we performed the LF experiment at 1.5 K. Should the relaxation arise from a weak static field, the size of this field is $B_{\rm loc} = \lambda/\gamma_\mu \simeq 1.2$ mT, where $\gamma_\mu = 135.5 \times 2\pi$ s^{-1} μT^{-1} is the gyromagnetic ratio for muons. Our LF data show that the relaxation persists in much higher fields, thus proving the dynamic nature of the Yb^{3+} pseudospins [40].

We also note that the characteristic evolution of λ_1, its increase below 10 K and the saturation below 2 K, takes place at about two times higher temperatures compared to $YbMgGaO_4$ [8]. This further supports our conclusion on the two times stronger exchange couplings in $NaYbO_2$.

D. Low-energy excitations probed by inelastic neutron scattering

The most interesting property of a spin liquid is arguably its excitation spectrum. We probed the low-energy excitations of $NaYbO_2$ at 45 mK using incident neutron energies of 1.46, 3.7, and 7.52 meV at the LET. Spectral weight observed above 0.8 Å^{-1} is continuously distributed in both energy E and momentum Q and extends to about 1 meV [see Fig. 5(a)]. This low-energy spectral weight concentrates around $Q \simeq 1.25$ Å^{-1}, which can be identified as the K point of the Brillouin zone with the reciprocal-lattice vector $(\frac{1}{3}, \frac{1}{3}, 0)$. A 120° magnetic order will lead to a Bragg peak at the same position, but the excitation spectrum is clearly different from the spin-wave spectrum of such an ordered state simulated using the SPINW software [40,51]. The energy dependence over the constant-Q cut suggests that the excitations reach low energies down to the elastic line that becomes prominent below 0.1 meV. This further confirms the gapless nature of the magnetic excitations in $NaYbO_2$ [see Fig. 5(b)]. Note that background-subtracted data using the raw data measured at 45 mK and 50 K give the same results.

The spectrum of $NaYbO_2$ has close similarities to that of $YbMgGaO_4$, where no spectral weight was observed at low Q, around the zone center, because spin-spin correlations are purely antiferromagnetic. All the spectral weight is concentrated in the vicinity of the zone boundary, in agreement with our observation of the spectral weight only above 0.8 Å^{-1}. On the other hand, the low-energy spectral weight for $YbMgGaO_4$ peaks at the M point ($Q \simeq 1.08$ Å^{-1}) [15], which is very different from $NaYbO_2$ with the peak at the Q value corresponding to the K point. Moreover, magnetic excitations in $YbMgGaO_4$ extend to the much higher energy of 2 meV, despite the fact that $\bar{J}_1$ is two times smaller than in $NaYbO_2$.

IV. DISCUSSION

$NaYbO_2$ shows several strong similarities to the widely studied triangular spin-liquid candidate $YbMgGaO_4$ but evades chemical site disorder that can influence the magnetism of $4f$ cations. Both materials entail the trigonally distorted YbO_6 octahedra. The CEF excitations of Yb^{3+} occur at about the same energies, and the compositions of the ground-state Kramers doublets are similar too. Exchange couplings differ by a factor of 2, however. This change is accompanied by a reduction in the Yb-O-Yb bridging angle from 99.4° in $YbMgGaO_4$ to 95.7° in $NaYbO_2$.

Rau and Gingras [52] computed anisotropic nearest-neighbor exchange couplings for several triangular geometries inspired by the possible local structures of $YbMgGaO_4$. By extrapolating their results to the Yb-O-Yb angle of 95.7° in $NaYbO_2$, we may expect that at least the nearest-neighbor coupling $\bar{J}_1$ in this material is very close to the Heisenberg limit. In fact, all our observations can then be understood even on the level of the Heisenberg model by assuming the second-neighbor coupling $\bar{J}_2$, with $\bar{J}_2/\bar{J}_1 = 0.13$–$0.15$, that, on the one hand, stabilizes the spin-liquid ground state with the spectral weight accumulated at the K point [32] but, on the other hand, triggers the 1/2 magnetization plateau [47]. This scenario looks even more plausible in light of the sizable $\bar{J}_2/\bar{J}_1 = 0.18(7)$ established in $YbMgGaO_4$ [15,19] and the fact that $\bar{J}_1$ increases upon reducing the Yb-O-Yb angle, whereas $\bar{J}_2$, as a long-range coupling, should be less sensitive to the structural changes. It may happen that $\bar{J}_2$ increases as well. However, $\bar{J}_1 \sim 3.8$ K will then lead to $\bar{J}_2$ of nearly 1 K, which is hard to reconcile with the second-neighbor Yb-Yb distance of 5.82 Å and the strongly localized nature of f electrons in Yb^{3+}.

Recent theoretical studies [20,21,32] suggest that this spin-liquid phase may be a Dirac QSL and should be

characterized by the peak of the low-energy spectral weight at the K points [32], consistent with our experimental observations. Additionally, our INS and specific-heat measurements indicate the gapless nature of this spin liquid, thus setting an important reference for theoretical studies. Other delafossite materials, including $NaYbS_2$ [36], may host similar QSLs, but their spin dynamics remains to be studied. $NaYbO_2$ is thus the first clear-cut manifestation of the theoretically predicted QSL state in triangular antiferromagnets. Its gapless nature and unusual sensitivity to the magnetic field open prospects for future studies theoretically and experimentally.

V. CONCLUSIONS

$NaYbO_2$ without chemical site disorder gives direct experimental access to the spin-liquid physics of the TL model. Thermodynamic measurements and muon spectroscopy indicate the absence of magnetic order and persistent spin dynamics down to at least 70 mK. An excitation continuum is observed. Its main features, including the accumulation of the spectral weight around $Q \simeq 1.25\,\text{Å}^{-1}$, are consistent with theoretical expectations for the QSL phase(s) driven by the exchange anisotropy or second-neighbor coupling on the TL model. The spin excitations of $NaYbO_2$ are gapless with a nontrivial low-temperature evolution of the specific heat, which does not follow the spinon scenario originally proposed for $YbMgGaO_4$.

ACKNOWLEDGMENTS

L.D. acknowledges support from the Rutherford International Fellowship Programme (RIFP). This project has received funding from the European Union's Horizon 2020 research and innovation program under Marie Skłodowska-Curie Grant Agreement No. 665593 awarded to the Science and Technology Facilities Council. R.D.J. acknowledges financial support from the Royal Society. The work in Augsburg was supported by the German Research Foundation (DFG) via Project No. 107745057 (TRR80). The magnetization measurements at high fields were performed at the National High Magnetic Field Laboratory, which is supported by National Science Foundation Cooperative Agreements No. DMR-1157490 and No. DMR-1644779 and the state of Florida, as well as the Strongly Correlated Magnets thrust of the DoE BES "Science in 100 T" program. L.D. thanks G. Stenning for his help during the thermodynamic measurements in the Materials Characterisation Laboratory and P. Biswas during the muon data collection at the ISIS facility. L.D. is grateful to M. D. Le for his help in using MANTID. A.T. thanks Y. Li, M. Majumder, M. Baenitz, L. Hozoi, and A. Chernyshev for useful discussions and ESRF for providing the beam time at ID22.

[1] L. Balents, Spin liquids in frustrated magnets, Nature (London) **464**, 199 (2010).
[2] L. Savary and L. Balents, Quantum spin liquids: A review, Rep. Prog. Phys. **80**, 016502 (2017).
[3] J. Knolle and R. Moessner, A field guide to spin liquids, Annu. Rev. Condens. Matter Phys. **10**, 451 (2019).
[4] P. W. Anderson, Resonating valence bonds: A new kind of insulator? Mater. Res. Bull. **8**, 153 (1973).
[5] O. A. Starykh, Unusual ordered phases of highly frustrated magnets: A review, Rep. Prog. Phys. **78**, 052502 (2015).
[6] Y. S. Li, H. J. Liao, Z. Zhang, S. Y. Li, F. Jin, L. S. Ling, L. Zhang, Y. M. Zou, L. Pi, Z. R. Yang, J. F. Wang, Z. H. Wu, and Q. M. Zhang, Gapless quantum spin liquid ground state in the two-dimensional spin-1/2 triangular antiferromagnet $YbMgGaO_4$, Sci. Rep. **5**, 16419 (2015).
[7] Y. Li, G. Chen, W. Tong, L. Pi, J. Liu, Z. Yang, X. Wang, and Q. Zhang, Rare-Earth Triangular Lattice Spin Liquid: A Single-Crystal Study of $YbMgGaO_4$, Phys. Rev. Lett. **115**, 167203 (2015).
[8] Y. S. Li, D. Adroja, P. K. Biswas, P. J. Baker, Q. Zhang, J. Liu, A. A. Tsirlin, P. Gegenwart, and Q. M. Zhang, Muon Spin Relaxation Evidence for the U(1) Quantum Spin-Liquid Ground State in the Triangular Antiferromagnet $YbMgGaO_4$, Phys. Rev. Lett. **117**, 097201 (2016).
[9] Y. Shen, Y. D. Li, H. L. Wo, Y. S. Li, S. D. Shen, B. Y. Pan, Q. S. Wang, H. C. Walker, P. Steffens, M. Boehm, Y. Q. Hao, D. L. Quintero-Castro, L. W. Harriger, M. D. Frontzek, L. J. Hao, S. Q. Meng, Q. M. Zhang, G. Chen, and J. Zhao, Evidence for a spinon Fermi surface in a triangular-lattice quantum-spin-liquid candidate, Nature (London) **540**, 559 (2016).
[10] Y. Shen, Y. D. Li, H. L. Wo, Y. S. Li, S. D. Shen, B. Y. Pan, Q. S. Wang, H. C. Walker, P. Steffens, M. Boehm, Y. Q. Hao, D. L. Quintero-Castro, L. W. Harriger, M. D. Frontzek, L. J. Hao, S. Q. Meng, Q. M. Zhang, G. Chen, and J. Zhao, Fractionalized excitations in the partially magnetized spin liquid candidate $YbMgGaO_4$, Nat. Commun. **9**, 4138 (2018).
[11] Y. S. Li, D. Adroja, D. Voneshen, R. I. Bewley, Q. M. Zhang, A. A. Tsirlin, and P. Gegenwart, Nearest-neighbour resonating valence bonds in $YbMgGaO_4$, Nat. Commun. **8**, 15814 (2017).
[12] I. Kimchi, A. Nahum, and T. Senthil, Valence Bonds in Random Quantum Magnets: Theory and Application to $YbMgGaO_4$, Phys. Rev. X **8**, 031028 (2018).
[13] Y. Li, S. Bachus, B. Liu, I. Radelytskyi, A. Bertin, A. Schneidewind, Y. Tokiwa, A. A. Tsirlin, and P. Gegenwart, Rearrangement of Uncorrelated Valence Bonds Evidenced by Low-Energy Spin Excitations in $YbMgGaO_4$, Phys. Rev. Lett. **122**, 137201 (2019).
[14] Y. Xu, J. Zhang, Y. S. Li, Y. J. Yu, X. C. Hong, Q. M. Zhang, and S. Y. Li, Absence of Magnetic Thermal Conductivity in the Quantum Spin-Liquid Candidate $YbMgGaO_4$, Phys. Rev. Lett. **117**, 267202 (2016).
[15] J. A. M. Paddison, M. Daum, Z. L. Dun, G. Ehlers, Y. H. Liu, M. B. Stone, H. D. Zhou, and M. Mourigal, Continuous excitations of the triangular-lattice quantum spin liquid $YbMgGaO_4$, Nat. Phys. **13**, 117 (2017).

[16] Y. S. Li, D. Adroja, R. I. Bewley, D. Voneshen, A. A. Tsirlin, P. Gegenwart, and Q. M. Zhang, Crystalline Electric-Field Randomness in the Triangular Lattice Spin-Liquid $YbMgGaO_4$, Phys. Rev. Lett. **118**, 107202 (2017).

[17] Z. Y. Zhu, P. A. Maksimov, S. R. White, and A. L. Chernyshev, Disorder-Induced Mimicry of a Spin Liquid in $YbMgGaO_4$, Phys. Rev. Lett. **119**, 157201 (2017).

[18] E. Parker and L. Balents, Finite-temperature behavior of a classical spin-orbit-coupled model for $YbMgGaO_4$ with and without bond disorder, Phys. Rev. B **97**, 184413 (2018).

[19] X. S. Zhang, F. Mahmood, M. Daum, Z. L. Dun, J. A. M. Paddison, N. J. Laurita, T. Hong, H. D. Zhou, N. P. Armitage, and M. Mourigal, Hierarchy of Exchange Interactions in the Triangular-Lattice Spin Liquid $YbMgGaO_4$, Phys. Rev. X **8**, 031001 (2018).

[20] J. Iaconis, C. Liu, G. B. Halasz, and L. Balents, Spin liquid versus spin orbit coupling on the triangular lattice, SciPost Phys. **4**, 003 (2018).

[21] P. A. Maksimov, Z.-Y. Zhu, S. R. White, and A. L. Chernyshev, Anisotropic-Exchange Magnets on a Triangular Lattice: Spin Waves, Accidental Degeneracies, and Dual Spin Liquids, Phys. Rev. X **9**, 021017 (2019).

[22] X.-Y. Song, C. Wang, A. Vishwanath, and Y.-C. He, Unifying description of competing orders in two dimensional quantum magnets, Nat. Commun. **10**, 4254 (2019).

[23] M. E. Zhitomirsky and A. L. Chernyshev, Colloquium: Spontaneous magnon decays, Rev. Mod. Phys. **85**, 219 (2013).

[24] R. Kaneko, S. Morita, and M. Imada, Gapless spin-liquid phase in an extended spin-1/2 triangular Heisenberg model, J. Phys. Soc. Jpn. **83**, 093707 (2014).

[25] W.-J. Hu, S.-S. Gong, W. Zhu, and D. N. Sheng, Competing spin-liquid states in the spin-$\frac{1}{2}$ Heisenberg model on the triangular lattice, Phys. Rev. B **92**, 140403(R) (2015).

[26] Z. Zhu and S. R. White, Spin liquid phase of the $S = 1/2 J_1 - J_2$ Heisenberg model on the triangular lattice, Phys. Rev. B **92**, 041105(R) (2015).

[27] R. F. Bishop and P. H. Y. Li, Spin-gap study of the spin-$\frac{1}{2} J_1 - J_2$ model on the triangular lattice, Europhys. Lett. **112**, 67002 (2015).

[28] Y. Iqbal, W.-J. Hu, R. Thomale, D. Poilblanc, and F. Becca, Spin liquid nature in the Heisenberg J_1-J_2 triangular antiferromagnet, Phys. Rev. B **93**, 144411 (2016).

[29] S. N. Saadatmand and I. P. McCulloch, Symmetry fractionalization in the topological phase of the spin-$\frac{1}{2} J_1$-J_2 triangular Heisenberg model, Phys. Rev. B **94**, 121111(R) (2016).

[30] D.-V. Bauer and J. O. Fjærestad, Schwinger-boson mean-field study of the J_1-J_2 Heisenberg quantum antiferromagnet on the triangular lattice, Phys. Rev. B **96**, 165141 (2017).

[31] S. N. Saadatmand and I. P. McCulloch, Detection and characterization of symmetry-broken long-range orders in the spin-$\frac{1}{2}$ triangular Heisenberg model, Phys. Rev. B **96**, 075117 (2017).

[32] Z. Y. Zhu, P. A. Maksimov, S. R. White, and A. L. Chernyshev, Topography of Spin Liquids on a Triangular Lattice, Phys. Rev. Lett. **120**, 207203 (2018).

[33] Y.-D. Li, Y.-M. Lu, and G. Chen, Spinon Fermi surface U(1) spin liquid in the spin-orbit-coupled triangular-lattice Mott insulator $YbMgGaO_4$, Phys. Rev. B **96**, 054445 (2017).

[34] Y.-D. Li and G. Chen, Detecting spin fractionalization in a spinon Fermi surface spin liquid, Phys. Rev. B **96**, 075105 (2017).

[35] Y.-D. Li, Y. Shen, Y.-S. Li, J. Zhao, and G. Chen, Effect of spin-orbit coupling on the effective-spin correlation in $YbMgGaO_4$, Phys. Rev. B **97**, 125105 (2018).

[36] M. Baenitz, P. Schlender, J. Sichelschmidt, Y. A. Onykiienko, Z. Zangeneh, K. M. Ranjith, R. Sarkar, L. Hozoi, H. C. Walker, J.-C. Orain, H. Yasuoka, J. van den Brink, H. H. Klauss, D. S. Inosov, and T. Doert, $NaYbS_2$: A planar spin-1/2 triangular-lattice magnet and putative spin liquid, Phys. Rev. B **98**, 220409(R) (2018).

[37] W. W. Liu, Z. Zhang, J. T. Ji, Y. X. Liu, J. S. Li, X. Wang, H. Lei, G. Chen, and Q. M. Zhang, Rare-earth chalcogenides: A large family of triangular lattice spin liquid candidates, Chin. Phys. Lett. **35**, 117501 (2018).

[38] L. C. Chapon, P. Manuel, P. G. Radaelli, C. Benson, L. Perrott, S. Ansell, N. J. Rhodes, D. D. Raspino, E. Spill, and J. Norris, Wish: The new powder and single crystal magnetic diffractometer on the second target station, Neutron News **22**, 22 (2011).

[39] R. I. Bewley, R. S. Eccleston, K. A. McEwen, S. M. Hayden, M. T. Dove, S. M. Bennington, J. R. Treadgold, and R. L. S. Coleman, MERLIN, a new high count rate spectrometer at ISIS, Phys. B (Amsterdam, Neth.) **385-386**, 1029 (2006).

[40] See Supplemental Material at http://link.aps.org/supplemental/10.1103/PhysRevB.100.144432 for an additional description of the experimental methods, crystal structure refinements, details of the CEF fit, and analysis of the low-temperature heat capacity.

[41] R. I. Bewley, J. W. Taylor, and S. M. Bennington, LET, a cold neutron multi-disk chopper spectrometer at ISIS, Nucl. Instrum. Methods Phys. Res., Sect. A **637**, 128 (2011).

[42] J. Rodríguez-Carvajal, Recent advances in magnetic structure determination by neutron powder diffraction, Phys. B (Amsterdam, Neth.) **192**, 55 (1993).

[43] J. Gaudet, D. D. Maharaj, G. Sala, E. Kermarrec, K. A. Ross, H. A. Dabkowska, A. I. Kolesnikov, G. E. Granroth, and B. D. Gaulin, Neutron spectroscopic study of crystalline electric field excitations in stoichiometric and lightly stuffed $Yb_2Ti_2O_7$, Phys. Rev. B **92**, 134420 (2015).

[44] K. A. Ross, L. Savary, B. D. Gaulin, and L. Balents, Quantum Excitations in Quantum Spin Ice, Phys. Rev. X **1**, 021002 (2011).

[45] O. Arnold, J. C. Bilheux, J. M. Borreguero, A. Buts, S. I. Campbell, L. Chapon, M. Doucet, N. Draper, R. Ferraz Leal, M. A. Gigg, V. E. Lynch, A. Markvardsen, D. J. Mikkelson, R. L. Mikkelson, R. Miller, K. Palmen, P. Parker, G. Passos, T. G. Perring, P. F. Peterson, S. Ren, M. A. Reuter, A. T. Savici, J. W. Taylor, R. J. Taylor, R. Tolchenov, W. Zhou, and J. Zikovsky, Mantiddata analysis and visualization package for neutron scattering and μSR experiments, Nucl. Instrum. Methods Phys. Res., Sect. A **764**, 156 (2014).

[46] Y.-D. Li, X. Wang, and G. Chen, Anisotropic spin model of strong spin-orbit-coupled triangular antiferromagnets, Phys. Rev. B **94**, 035107 (2016).

[47] M.-X. Ye and A. V. Chubukov, Half-magnetization plateau in a Heisenberg antiferromagnet on a triangular lattice, Phys. Rev. B **96**, 140406(R) (2017).

[48] K. M. Ranjith, D. Dmytriieva, S. Khim, J. Sichelschmidt, S. Luther, D. Ehlers, H. Yasuoka, J. Wosnitza, A. A. Tsirlin, H. Kühne, and M. Baenitz, Field-induced instability of the quantum spin liquid ground state in the $J_{\text{eff}} = 1/2$ triangular-lattice compound $NaYbO_2$, Phys. Rev. B **99**, 180401(R) (2019).

[49] Y. S. Li, S. Bachus, Y. Tokiwa, A. A. Tsirlin, and P. Gegenwart, Gapped ground state in the zigzag pseudospin-1/2 quantum antiferromagnetic chain compound $PrTiNbO_6$, Phys. Rev. B **97**, 184434 (2018).

[50] O. I. Motrunich, Variational study of triangular lattice spin-1/2 model with ring exchanges and spin liquid state in κ-$(ET)_2Cu_2(CN)_3$, Phys. Rev. B **72**, 045105 (2005).

[51] S. Toth and B. Lake, Linear spin wave theory for single-Q incommensurate magnetic structures, J. Phys.: Condens. Matter **27**, 166002 (2015).

[52] J. G. Rau and M. J. P. Gingras, Frustration and anisotropic exchange in ytterbium magnets with edge-shared octahedra, Phys. Rev. B **98**, 054408 (2018).